



(RESEARCH ARTICLE)



## Mechanical performance study of high flexibility arrow-shaped concave arc bottoms negative Poisson's ratio honeycomb structure

Ding Shuangjiang <sup>1,\*</sup>, Song Leipeng <sup>2</sup>, Wang Taoxi <sup>1</sup> and Shen Xing <sup>1</sup>

<sup>1</sup> Nanjing University of Aeronautics and Astronautics, Nanjing 210016, China.

<sup>2</sup> Zhejiang University of Science and Technology, Hangzhou, 310023, China.

International Journal of Science and Research Archive, 2024, 13(01), 2122–2135

Publication history: Received on 23 August 2024; revised on 04 October 2024; accepted on 06 October 2024

Article DOI: <https://doi.org/10.30574/ijrsra.2024.13.1.1882>

### Abstract

A novel negative Poisson's ratio honeycomb structure with arrow-shaped concave arc bottoms was presented in this paper. The analytical formulas for the equivalent elastic modulus, equivalent Poisson's ratio, and equivalent density were derived based on the theory of the Timoshenko beam under small static deformations and verified by experiments and finite element simulations. Comparative analysis with common negative Poisson's ratio honeycomb structures revealed that the arrow-shaped concave arc bottom structure exhibits superior deformability under load. Experimental results showed that the elastic modulus of the structure is only 5.34% of that of the classical concave hexagonal structure. Furthermore, a parametric analysis systematically investigated the influence of geometric parameters on the structural in-plane equivalent mechanical properties, which can provide some guidance for the parameter design of the honeycomb structure in practical application.

**Keywords:** Negative Poisson's ratio honeycomb structure; Arrow-shaped concave-arc bottom cell; Energy method; Effective mechanical properties; Parameter analysis

### 1. Introduction

Negative Poisson's ratio (NPR) materials, also known as auxetic materials, expand laterally when subjected to tensile stress<sup>[1]</sup>. Due to their advantageous properties, such as enhanced shear resistance, fracture toughness, porosity, and energy absorption, NPR materials have garnered significant research interest<sup>[2]</sup>. Early reports of NPR effects date back to the early 20th century, when chemists identified this phenomenon in natural substances like pyrite, arsenic, cadmium, and ferromagnetic films. In 1987, Lakes<sup>[7]</sup> successfully fabricated the first synthetic NPR material by treating polyurethane foam, achieving a Poisson's ratio of -0.7. In 1989, Evans et al. <sup>[8]</sup> further demonstrated the NPR effect in microporous polytetrafluoroethylene (PTFE) structures, coining the term "auxetic materials."

The negative Poisson's ratio (NPR) honeycomb structure, a typical auxetic design, is formed by the periodic arrangement of specific unit cells. Due to its low weight, ease of fabrication, and excellent mechanical properties, various types of unit cells have been extensively studied. Among the different NPR honeycomb structures, the concave hexagonal configuration is the most representative. Gibson et al. <sup>[9]</sup> were the first to derive theoretical expressions for mechanical parameters such as Poisson's ratio, elastic modulus, and shear modulus for hexagonal honeycomb structures under compressive loads. Building on Gibson et al.'s work, many researchers have further explored the influence of geometric parameters, including wall thickness, edge length, and cell inclination angle, on the static plateau stress and energy absorption of hexagonal honeycomb structures<sup>[10]</sup>.

Many researchers have proposed novel unit cell structures and analyzed their mechanical properties. Li et al.<sup>[13]</sup> introduced two sinusoidal ribs into the classical re-entrant topology, demonstrating that these new configurations

\* Corresponding author: Ding Shuangjiang

exhibit superior energy absorption compared to traditional designs. Ren Yiru et al. [14], inspired by the concentric cellular structure of coconut trees, proposed a bio-inspired negative Poisson's ratio structure and conducted a detailed numerical study of its performance under impact conditions. Wang Liang and Liu Haitao [15] developed an X-shaped concave honeycomb structure and used numerical simulations to investigate its mechanical properties. Guo Zhixi [16] introduced a multi-arc concave unit cell with adjustable Poisson's ratio characteristics, allowing the Poisson's ratio to be tuned between positive, zero, and negative values. Yang Hang et al. [17] designed dual U-shaped, finely-cracked auxetic materials with programmable tensile properties. Chang Lulu [18] applied topology optimization to create optimized honeycomb configurations aimed at reducing stiffness in the wing deformation direction. Yang Zhenyu's research group [19] combined star-shaped and double-arrowhead honeycomb microstructures to propose a novel auxetic model, the Star-Arrowhead Honeycomb (SAH). Numerical simulations revealed that SAH exhibited superior deformation characteristics and energy absorption compared to star-shaped honeycombs under various impact conditions. Song Leipeng [20] investigated the in-plane and out-of-plane mechanical properties of honeycomb structures, proposing theoretical methods to calculate the in-plane tensile modulus, in-plane shear modulus, and out-of-plane bending modulus. He also analyzed the influence of honeycomb geometry on their in-plane and out-of-plane mechanical performance.

Additionally, many researchers have proposed novel unit cell structures and analyzed their mechanical properties. Li et al. [13] innovatively introduced two sinusoidal ribs into the classical re-entrant topology, demonstrating that these new configurations exhibit superior energy absorption capacity compared to traditional re-entrant designs. Ren Yiru et al. [14], inspired by the concentric cellular structure of coconut trees, creatively proposed a bio-inspired negative Poisson's ratio structure and conducted an in-depth numerical study of its performance under impact conditions. Wang Liang and Liu Haitao [15] proposed an X-shaped concave honeycomb structure and then employed numerical simulation methods to investigate its mechanical properties. Guo Zhixi [16] introduced a multi-arc concave unit cell with adjustable Poisson's ratio characteristics, where the Poisson's ratio can be tuned between positive, zero, and negative values. Yang Hang et al. [17] designed a class of dual U-shaped, finely-cracked auxetic deformable materials with programmable tensile properties. Chang Lulu [18] applied topology optimization to design various optimized honeycomb-based configurations aimed at reducing stiffness in the wing deformation direction. The research group of Yang Zhenyu [18] combined star-shaped and double-arrowhead honeycomb microstructures to propose a novel auxetic honeycomb model, SAH (Star-Arrowhead Honeycomb). Numerical simulations revealed that SAH exhibited better deformation characteristics and energy absorption performance compared to star-shaped honeycombs under different impact conditions. Song Leipeng [20] investigated the in-plane and out-of-plane mechanical properties of honeycomb structures and proposed theoretical methods to calculate the in-plane tensile modulus, in-plane shear modulus, and out-of-plane bending modulus for cellular structures. He also analyzed the influence of honeycomb geometry on their in-plane and out-of-plane mechanical performance.

However, under certain application conditions, existing negative Poisson's ratio (NPR) structures often exhibit relatively high equivalent stiffness in the loading direction, which limits their practical applications. For instance, in the flexible skins of morphing wings, unit cell structures require a high degree of flexibility to enable smooth transitions between different airfoil shapes. In impact protection devices, excessive stiffness can prevent honeycomb structures from quickly entering the plastic region, thereby reducing their energy absorption capacity. To address these limitations, this paper proposes a novel NPR unit cell with enhanced flexibility. Theoretical expressions for its equivalent elastic modulus and Poisson's ratio were derived using the energy method. Finite element analysis and experimental validation were then performed to confirm the accuracy of these expressions. A comparison with the equivalent modulus of conventional NPR structures is also presented, followed by a discussion on the influence of geometric parameters on the mechanical properties of the proposed structure.

---

## 2. Cellular structure

Figure 1 illustrates the arrow-shaped concave-arc-bottom honeycomb structure and its representative unit cell. The unit cell consists of four straight edges, one curved edge, and one connecting line, exhibiting symmetry along the vertical axis. As shown in the figure,  $L_1$  denotes the length of wall  $AB$ ,  $L_2$  represents the length of wall  $BC$ ,  $h$  indicates the total height of the unit cell in the  $y$ -direction, and  $R$  denotes the radius of the concave arc  $FE$  at the bottom. The angles  $\theta_1$  and  $\theta_2$  represent the angles between walls  $AB$ ,  $BC$ , and the symmetry axis, respectively. The angle  $\alpha$  corresponds to the arc angle of the curved edge  $DC$ , where the extension of  $AB$  meets at point  $E$ , and  $DG$  represents the connecting wall of the cell. Assuming that all cell walls have homogeneous rectangular cross-sections,  $a$  is the thickness of the cell walls, and  $b$  is the depth of the cell walls.

The mechanical properties of the unit cell can be determined by seven parameters:  $L_1$ 、 $\theta_1$ 、 $\theta_2$ 、 $R$ 、 $h$ 、 $a$  , and  $b$  . Based on the structural dimension constraints,  $L_2$  and  $\alpha$  are treated as dependent parameters to facilitate subsequent theoretical derivation.

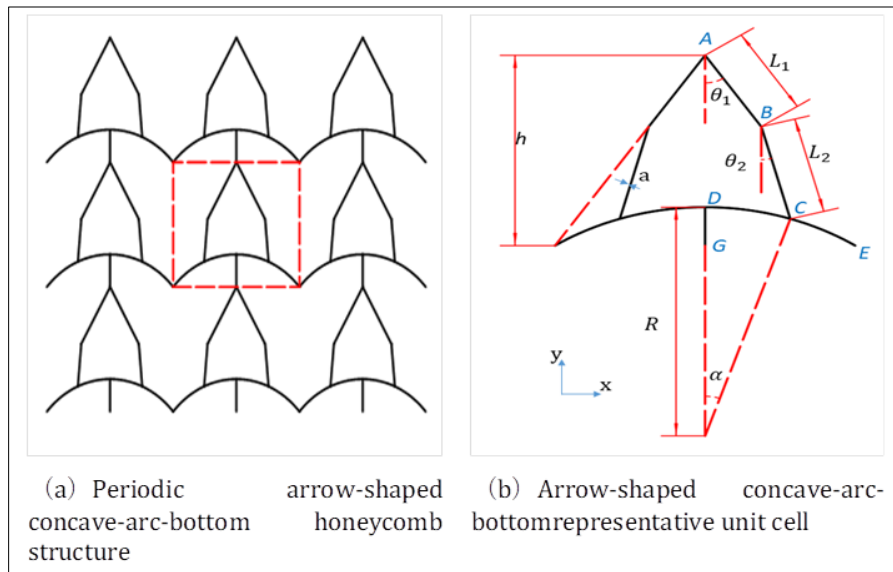


**Figure 1** The arrow-shaped concave-arc-bottom structure

## 2 Cellular density

The relative density of the structure is defined as the ratio of the equivalent density of the unit cell to the density of the base material, with values ranging from 0 to 1. The formula for calculating the relative density is given by [Error! Reference source not found.](#);

$$\rho = \frac{A_s}{A_\alpha} = \frac{2(L_1 + L_2) + 2R \arcsin(h \tan \theta_1 / R) + R - R \sqrt{1 - (h \tan \theta_1 / R)^2}}{2h^2 \tan \theta_1 / a} \tag{1}$$

In this context,  $A_s$  represents the area occupied by the wall panels of the representative unit cell, while  $A_\alpha$  denotes the effective total area of the wall panels in the unit cell.

## 3. Mechanical performance analysis

Before analyzing the mechanical properties of the functional unit, the following basic assumptions are made:

- The walls of the unit cell are considered uniform slender beams, and the structural material exhibits a homogeneous elastic modulus under stress conditions, denoted as  $E$  ;
- The material is assumed to deform within the range of isotropic elastic deformation, allowing the application of beam theory to determine the equivalent elastic modulus of the structural base material.
- All connection points between the functional units in the honeycomb structure are assumed to be rigid connections.

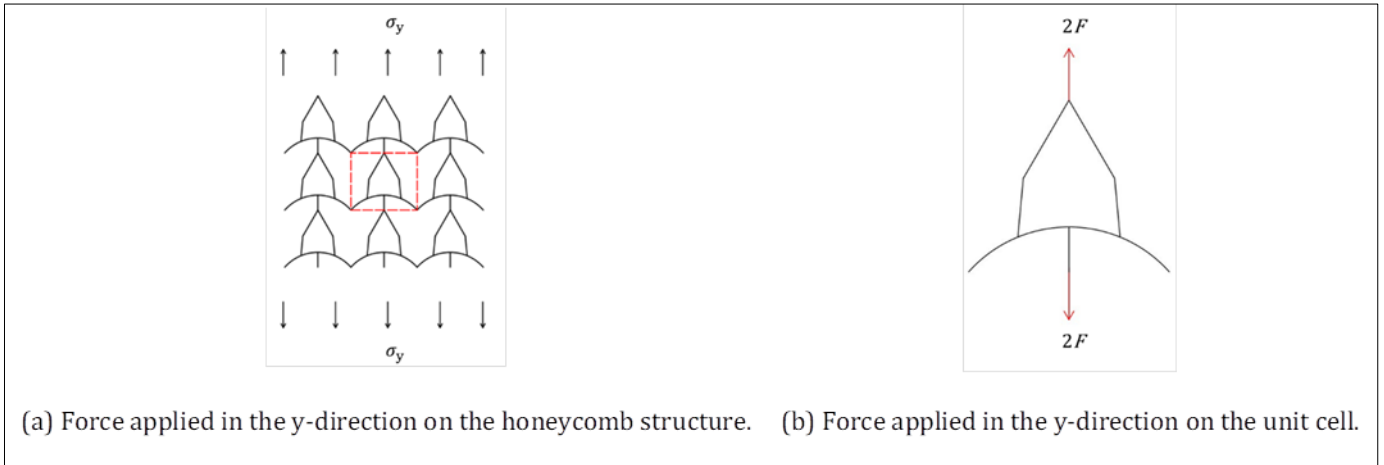
### 3.1. Theoretical derivation

Figure 2(a) illustrates the schematic diagram of the periodic arrow-shaped concave-arc-bottom honeycomb structure subjected to tensile stress in the y-direction, where  $\sigma_y$  represents the tensile stress along this axis, and the structure is in the elastic deformation stage. As shown in Figure 2(b), a representative unit cell is extracted from the periodic structure for mechanical analysis:

$$F = \sigma_y A_y \dots\dots\dots(2)$$

$$A_y = bh \tan \theta \dots\dots\dots(3)$$

where  $A_y$  represents the total finite cross-sectional area in the y-direction of half of the unit cell.



**Figure 2** Schematic diagram of the force applied on the arrow-shaped concave-arc-bottom honeycomb structure

Assuming that the walls of the unit cell are uniform slender beams and that the structural material exhibits an effective elastic modulus and equivalent Poisson's ratio under stress conditions, it is further assumed that the material deforms within the range of isotropic linear elasticity. Consequently, beam theory can be utilized to determine the equivalent elastic modulus of the composite material that composes the structure, denoted as  $E$ . Due to the symmetry of the unit cell, it is sufficient to consider only half of the structure, as shown in Figure 3.

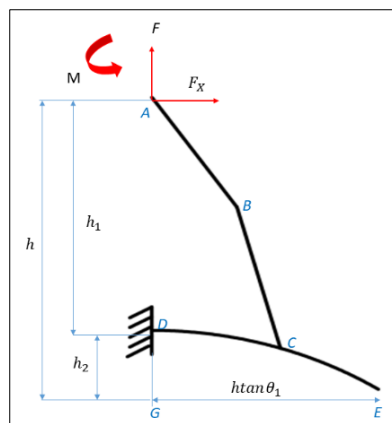


**Figure 3** Schematic diagram of the force applied on half of the unit cell

By utilizing the properties of this symmetric structure, it can be determined that the problem represents a second-order hyperstatic structure. In the diagram,  $F$  represents half of the external load in the y-direction, while  $F_x$  and  $M$  denote the symmetric constraint loads.  $h_1$  and  $h_2$  are the heights of segments  $AD$  and  $DG$ , respectively.

This symmetric structure must satisfy the displacement compatibility equation relating the x-direction displacement and the rotation about this plane, represented by Equation (4). The symmetric loads  $F_x$  and  $M$  can be calculated based on Equation (4).

$$\begin{cases} \Delta_{F\theta_A} + \delta_{11}M + \delta_{12}F_x = 0 \\ \Delta_{FX_A} + \delta_{21}M + \delta_{22}F_x = 0 \end{cases} \dots\dots\dots(4)$$

Where:  $\delta_{11}$  represents the rotation at point A caused by a unit moment applied at point A (with counterclockwise direction defined as positive),  $\delta_{12}$  denotes the rotation at point A caused by a unit force applied in the x-direction.  $\delta_{21}$  represents the x-direction displacement at point A due to a unit moment applied at point A, and  $\delta_{22}$  denotes the x-direction displacement at point A caused by a unit force applied in the x-direction.  $\Delta_{F\theta_A}$  indicates the rotation at point A due to the sole action of the force  $F$ , and  $\Delta_{FX_A}$  represents the displacement along the x-direction at point A due to the sole action of the force  $F$ . Using the moment integral method,  $\delta_{11}$ 、 $\delta_{12}$ 、 $\delta_{22}$ 、 $\Delta_{F\theta_A}$  and  $\Delta_{FX_A}$  can be determined.

$$\delta_{11} = \int_0^{L_1} \frac{1}{EI} dx + \int_0^{L_2} \frac{1}{EI} dx + \int_0^\alpha \frac{1}{EI} R d\phi = \frac{1}{EI} (L_1 + L_2 + R\alpha) \dots\dots\dots(5)$$

$$\begin{aligned} \delta_{12} = \delta_{21} &= \int_0^{L_1} \frac{(-1) \bullet (xcos\theta_1)}{EI} + \int_0^{L_2} \frac{(-1) \bullet (L_1cos\theta_1 + xcos\theta_2)}{EI} + \int_0^\alpha \frac{(-1) \bullet (h_1 + R - Rcos\alpha)}{EI} d\phi \\ &= \frac{-1}{2EI} (L_1^2cos\theta_1 + 2L_1L_2cos\theta_1 + L_2^2cos\theta_2) + \frac{-R^2}{EI} [(h_1 + R)\alpha - Rsin\alpha] \end{aligned} \dots\dots\dots(6)$$

$$\begin{aligned} \delta_{22} &= \int_0^{L_1} \frac{(xcos\theta_1)^2}{EI} + \int_0^{L_2} \frac{(L_1cos\theta_1 + xcos\theta_2)^2}{EI} + \int_0^\alpha \frac{(h_1 + R - Rcos\alpha)^2}{EI} d\phi \\ &= \frac{1}{3EI} (L_1^3cos^2\theta_1 + 3L_1^2L_2cos^2\theta_1 + 3L_1L_2^2cos\theta_1cos\theta_2 + L_2^3cos^2\theta_2) \\ &\quad + \frac{1}{EA} (L_1sin^2\theta_1 + L_2sin^2\theta_2) \\ &\quad + \frac{R^2}{EI} [(h_1 + R)^2\alpha - 2(h_1 + R)Rsin\alpha + R^2(\frac{1}{4}sin2\alpha + \frac{\alpha}{2})] \end{aligned} \dots\dots\dots(7)$$

$$\begin{aligned} \Delta_{F\theta_A} &= \int_0^{L_1} \frac{F \bullet (xsin\theta_1) \bullet (-1)}{EI} + \int_0^{L_2} \frac{F \bullet (L_1sin\theta_1 + xsin\theta_2) \bullet (-1)}{EI} + \int_0^\alpha \frac{F \bullet (sin\phi) \bullet (-1)}{EI} R d\phi \\ &= \frac{-F}{2EI} (L_1^2sin\theta_1 + 2L_1L_2sin\theta_1 + L_2^2sin\theta_2) + \frac{-FR^2}{EI} (1 - cos\alpha) \end{aligned} \dots\dots\dots(8)$$

$$\begin{aligned} \Delta_{FX_A} &= \int_0^{L_1} \frac{F \bullet (xcos\theta_1) \bullet (xsin\theta_1)}{EI} + \int_0^{L_2} \frac{F \bullet (L_1cos\theta_1 + xcos\theta_2) \bullet (L_1sin\theta_1 + xsin\theta_2)}{EI} + \int_0^\alpha \frac{F \bullet (sin\phi) \bullet (h_1 + R - Rcos\phi)}{EI} R d\phi \\ &\quad + \int_0^{L_1} \frac{cos\theta_1 \bullet (-sin\theta_1)}{EA} + \int_0^{L_2} \frac{cos\theta_2 \bullet (-sin\theta_2)}{EA} \\ &= \frac{F}{3EI} (L_1^3sin\theta_1cos\theta_1 + 3L_1^2L_2sin\theta_1cos\theta_1 + \frac{3}{2}L_1L_2^2sin\theta_1cos\theta_2 + \frac{3}{2}L_1L_2^2cos\theta_1sin\theta_2 + L_2^3sin\theta_2cos\theta_1) \\ &\quad - \frac{F}{EA} (L_1sin\theta_1cos\theta_1 + L_2sin\theta_2cos\theta_2) + \frac{FR^2}{EI} [h_1(1 - cos\alpha) + R(0.75 - cos\alpha + \frac{1}{4}cos2\alpha)] \end{aligned} \dots\dots\dots(9)$$

Where  $E$  is the elastic modulus of the material, and  $I$  is the moment of inertia of the rectangular cross-section about the neutral axis. By substituting Equations (5) to (9) into Equation (4), the constraint loads  $F_x$  and  $M$  can be solved.

$$Y_A = \Delta_{FY_A} + \Delta_{MY_A} + \Delta_{F_xY_A} \dots\dots\dots(10)$$

$$X_E = \Delta_{FX_E} + \Delta_{MX_E} + \Delta_{F_xX_E} \dots\dots\dots(11)$$

Where  $Y_A$  represents the longitudinal deformation of the functional unit (i.e., the displacement of point A in the y-direction under the action of external forces), and  $X_E$  denotes the lateral deformation of the functional unit (i.e., the displacement of point E in the x-direction under the action of external forces). In Equation (10),  $\Delta_{FY_A}$ 、 $\Delta_{MY_A}$  and  $\Delta_{F_x Y_A}$  represent the displacements of point A in the y-direction due to the individual actions of the moment  $F$ 、 $M$  and  $F_x$ , respectively. In Equation (11),  $\Delta_{FX_E}$ 、 $\Delta_{MX_E}$  and  $\Delta_{F_x X_E}$  represent the displacements of point E in the x-direction due to the individual actions of the moment  $F$ 、 $M$  and  $F_x$ , respectively.

Using the moment integral method, the calculation formulas for  $\Delta_{FY_A}$ 、 $\Delta_{MY_A}$  and  $\Delta_{F_x Y_A}$  can be obtained as follows:

$$\begin{aligned} \Delta_{FY_A} &= \int_0^{L_1} \frac{F}{EI} (x \sin \theta_1)^2 dx + \int_0^{L_2} \frac{F}{EI} (L_1 \sin \theta_1 + x \sin \theta_2)^2 dx + \int_0^{L_1} \frac{F}{EA} (\cos \theta_1)^2 dx \\ &+ \int_0^{L_2} \frac{F}{EA} (\cos \theta_2)^2 dx + \int_0^{\alpha} \frac{F}{EI} (R \sin \phi)^2 R d\phi \\ &= \frac{F}{3EI} (L_1^3 \sin^2 \theta_1 + 3L_1^2 L_2 \sin^2 \theta_1 + 3L_1 L_2^2 \sin \theta_1 \sin \theta_2 + L_2^3 \sin^2 \theta_2) \\ &+ \frac{F}{EA} (L_1 \cos^2 \theta_1 + L_2 \cos^2 \theta_2) + \frac{FR^3}{EI} \left( \frac{\alpha}{2} - \frac{1}{4} \sin \alpha \right) \end{aligned} \dots\dots\dots(12)$$

$$\begin{aligned} \Delta_{MY_A} &= \int_0^{L_1} \frac{M}{EI} (x \sin \theta_1) \square(-1) dx + \int_0^{L_2} \frac{M}{EI} (L_1 \sin \theta_1 + x \sin \theta_2) \square(-1) dx \\ &+ \int_0^{\alpha} \frac{M}{EI} (R \sin \phi) \square(-1) R d\phi \quad \dots\dots\dots(13) \\ &= -\frac{M}{2EI} (L_1^2 \sin \theta_1 + 2L_1 L_2 \sin \theta_1 + L_2^2 \sin \theta_2) - \frac{MR^2}{EI} (1 - \cos \alpha) \end{aligned}$$

$$\begin{aligned} \Delta_{F_x Y_A} &= \int_0^{L_1} \frac{F_x \bullet (x \cos \theta_1) \square(x \sin \theta_1)}{EI} dx + \int_0^{L_2} \frac{F_x \bullet (L_1 \cos \theta_1 + x \cos \theta_2) \bullet (L_1 \sin \theta_1 + x \sin \theta_2)}{EI} dx \\ &+ \int_0^{\alpha} \frac{F_x \bullet (\sin \phi) \square(h_1 + R - R \cos \phi)}{EI} R d\phi + \int_0^{L_1} \frac{\cos \theta_1 \bullet (-\sin \theta_1)}{EA} dx + \int_0^{L_2} \frac{\cos \theta_2 \bullet (-\sin \theta_2)}{EA} dx \\ &= \frac{F_x}{3EI} (L_1^3 \sin \theta_1 \cos \theta_1 + 3L_1^2 L_2 \sin \theta_1 \cos \theta_1 + \frac{3}{2} L_1 L_2^2 \sin \theta_1 \cos \theta_2 \\ &+ \frac{3}{2} L_1 L_2^2 \cos \theta_1 \sin \theta_2 + L_2^3 \sin \theta_2 \cos \theta_1) - \frac{F_x}{EA} (L_1 \sin \theta_1 \cos \theta_1 + L_2 \sin \theta_2 \cos \theta_2) \\ &+ \frac{F_x R^2}{EI} [h_1 (1 - \cos \alpha) + R(0.75 - \cos \alpha + \frac{1}{4} \cos 2\alpha)] \end{aligned} \dots\dots\dots(14)$$

Similarly, using the moment integral method, the calculation formulas for  $\Delta_{FX_E}$ 、 $\Delta_{MX_E}$  and  $\Delta_{F_x X_E}$  can be obtained as follows:

$$\begin{aligned} \Delta_{FX_E} &= \int_0^{\alpha} \frac{F}{EI} (R \sin \phi) \square[h_2 - R(1 - \cos \phi)] R d\phi \quad \dots\dots\dots(15) \\ &= \frac{R^2}{EI} [(h_2 - R)(1 - \cos \alpha) + 0.25R(1 - \cos 2\alpha)] \end{aligned}$$

$$\Delta_{MY_A} = \int_0^{\alpha} \frac{M}{EI} [h_2 - R(1 - \cos \phi)] R d\phi = \frac{MR}{EI} [(h_2 - R)\alpha + R \sin \alpha] \quad \dots\dots\dots(16)$$

$$\begin{aligned} \Delta_{F_x X_E} &= \int_0^\alpha \frac{F}{EI} (h_1 + R - R \cos \phi) [h_2 - R(1 - \cos \phi)] R d\phi \\ &= \frac{-R}{EI} [(h_2 - R)(h_1 + R)\alpha + (h_1 + 2R - h_2)R \sin \alpha - R^2 (\frac{1}{4} \sin 2\alpha + \frac{1}{2} \alpha)] \end{aligned} \quad \dots\dots\dots(17)$$

**3.2. Equivalent elastic modulus**

The equivalent elastic modulus of the honeycomb structure in the y-direction can be calculated using the equivalent stress  $E_e$  and the equivalent strain  $\sigma_y$  as follows:

$$\sigma_y = \frac{F}{bh \tan \theta_1} \quad \dots\dots\dots(18)$$

$$\varepsilon_y = \frac{Y_A}{h} \quad \dots\dots\dots(19)$$

$$E_e = \frac{\sigma_y}{\varepsilon_{x1}} \quad \dots\dots\dots(20)$$

By simultaneously solving Equations (10), (19), (18), and (20), the equivalent elastic modulus  $E_e$  of the topology-optimized honeycomb structure in the y-direction can be determined. Since all linear equations in the above process contain the common factor  $F$ , the final expression for the equivalent elastic modulus will result in the numerator and denominator canceling out  $F$ . Consequently, the final equivalent elastic modulus will be independent of the external force  $F$  and will depend solely on the geometric parameters that define the unit cell configuration.

This characteristic emphasizes that the mechanical performance of the optimized honeycomb structure is intrinsically linked to its geometric design rather than the magnitude of the applied load, which is a critical consideration in the design and application of such materials.

**3.3. Equivalent Poisson's ratio**

The equivalent Poisson's ratio of the honeycomb structure can be calculated using the equivalent strain  $\varepsilon_y$  and  $\varepsilon_x$  as follows

$$\varepsilon_x = \frac{X_E}{h \tan \theta_1} \quad \dots\dots\dots(21)$$

$$\nu_e = -\frac{\varepsilon_x}{\varepsilon_y} \quad \dots\dots\dots(22)$$

By simultaneously solving Equations (10), (11), (21), and (22), the equivalent Poisson's ratio of the topology-optimized honeycomb structure can be determined. Notably, since all linear equations in this process contain the common factor  $F$ , the final express  $F$  in both the numerator and denominator.

Consequently, the final equivalent Poisson's ratio is independent of the external force  $F$  and depends solely on the geometric parameters that define the unit cell configuration. This characteristic indicates that the mechanical behavior of the optimized honeycomb structure—particularly its ability to deform laterally in response to axial loading—is fundamentally governed by its design parameters rather than the magnitude of the applied load. This insight is essential for engineers and designers when creating materials that require specific mechanical properties for various applications.

#### 4. Finite element analysis and experimental validation

To validate the correctness of the theoretical model, this study utilizes the commercial software ABAQUS to conduct finite element simulations of a single unit cell. The BEAM33 element is selected for the analysis due to its suitability for simulating slender components and its ability to model third-order variables along the length direction, allowing for high accuracy with fewer elements.

Figure 4 illustrates the loading and boundary conditions of the arrow-shaped concave arc-bottom unit cell in the finite element model. The specific boundary conditions are as follows: the lower vertex is fixed, restricting its displacement in the x and y directions as well as its rotation, while a load is applied to the upper vertex in the direction parallel to the y-axis. The wall thickness of the unit cell used in this study is 1 mm, with the material's elastic modulus  $E$  set at 200,000 MPa and a Poisson's ratio of 0.3. The geometric parameters for modeling are based on those shown in Table 1, with the dimensions of the arrow-shaped concave arc-bottom unit cell varying from 10 mm to 30 mm, in increments of 1 mm. This comprehensive approach enables a thorough comparison between the theoretical predictions and the finite element simulation results, providing a robust foundation for validating the accuracy and reliability of the proposed model.

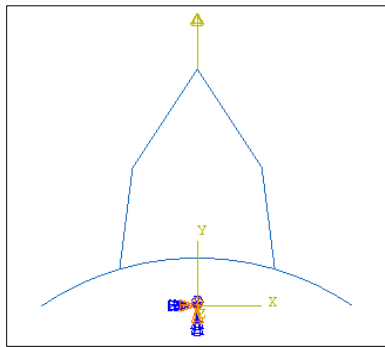


**Figure 4** Finite Element Model of the Arrow-Shaped Concave Arc-Bottom Unit Cell

**Table 1** Values of Geometric Parameters

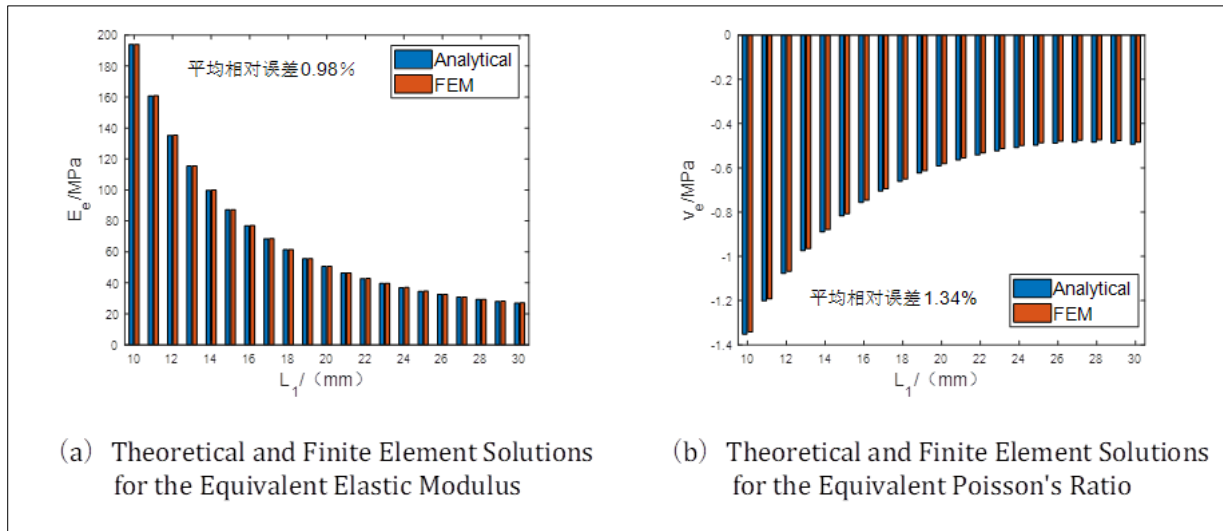
$L_1$ (mm)	$R$ (mm)	$h$ (mm)	$\theta_1$ ( $^\circ$ )	$\theta_2$ ( $^\circ$ )	$b$ (mm)
15	36	30	34	8	5

Define the relative error  $Error(\%)$  as:

$$Error(\%) = \frac{|\omega_{theoretical} - \omega_{FEM}|}{\omega_{theoretical}} \times 100\%$$

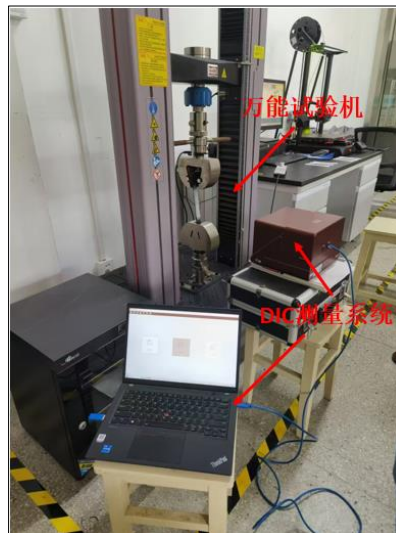
where  $\omega_{theoretical}$  is the theoretical solution and  $\omega_{FEM}$  is the finite element solution.

Figure 5 shows a comparison between the theoretical solutions and finite element results for the equivalent mechanical properties of the concave arrow-shaped honeycomb structure. The results indicate that the theoretical solutions are very close to the finite element simulation results, with an average relative error of only 0.98% for the equivalent elastic modulus and an average relative error of just 1.34% for the equivalent Poisson's ratio. These relative errors are all below 1.5%, effectively demonstrating the accuracy of the theoretical solutions.



**Figure 5** Comparison of Theoretical Solutions and Finite Element Results for the Equivalent Mechanical Properties of the Concave Arrow-Shaped Honeycomb Structure

In the previous sections, this study has conducted a theoretical analysis and finite element validation of the equivalent elastic modulus and equivalent Poisson's ratio for the cellular structure. However, to further validate these results, experimental verification is also necessary. This research utilized the XTDIC deformation measurement and analysis system, as shown in Figure 6. This non-contact optical measurement system is primarily applied in material testing, such as measuring Young's modulus, Poisson's ratio, and elastoplastic parameters; component testing, for measuring displacement and strain; finite element analysis (FEA) validation; and high-speed deformation measurement.



**Figure 6** DIC Deformation Measurement and Analysis System

After setting up the DIC measurement system and experimental apparatus, the experiment can commence by applying speckles to the sample and calibrating the camera. This equipment accurately analyzes the displacements and strains on the object's surface, generating cloud maps of the displacement and strain fields. The test sample of the arrow-shaped concave arch-bottom cellular unit, as shown in Figure 7, was 3D printed using R4600 resin (which has a tensile strength of 38 MPa, a tensile modulus of  $2700 \pm 20$  MPa, and a Poisson's ratio of 0.4–0.44). The geometric dimensions of the tested samples are consistent with those used in the finite element simulation, as listed in Table 1. The experiment measures the y-direction displacement of measurement point 1 after stretching, along with the x-direction displacements of measurement points 2 and 3. The equivalent Poisson's ratio and equivalent elastic modulus of the sample are calculated using formulas (20) and (22).

Figure 8 presents the DIC image analysis results for the arrow-shaped concave arch-bottom cellular unit sample after stretching. It can be observed that when the y-direction displacement of measurement point 1 is positive, the x-direction displacement of measurement point 3 is also positive. This indicates that the structure exhibits a certain degree of auxetic effect. Figures 9 and 10 display the variation of the equivalent Poisson's ratio of the arrow-shaped concave arch-bottom cellular unit sample over time and the stress-strain curve, respectively.

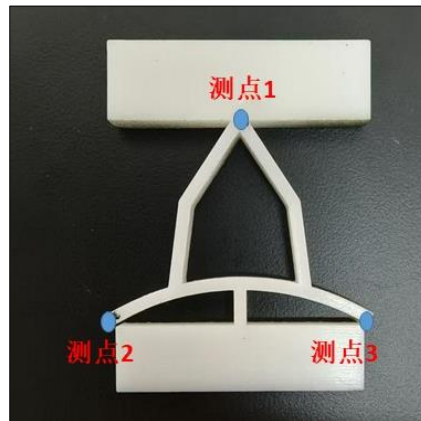


Figure 7 Arrow-shaped concave arch-bottom cellular unit sample

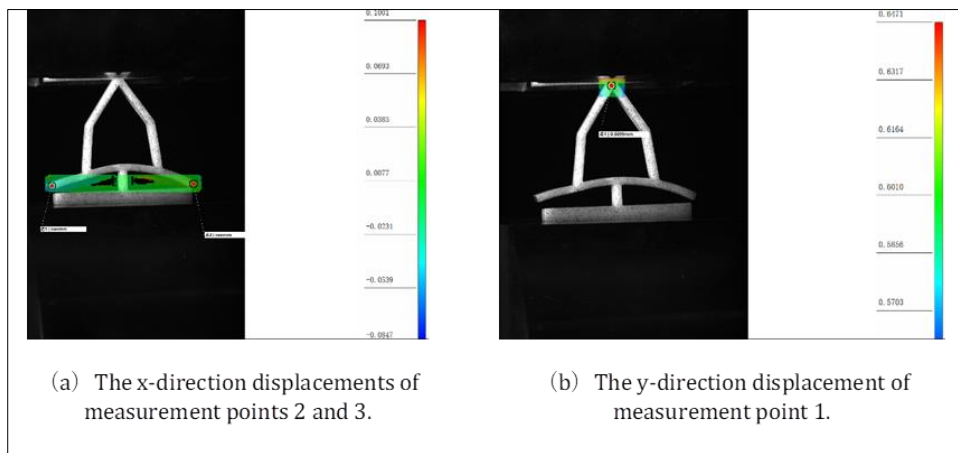


Figure 8 The DIC image analysis results of the arrow-shaped concave arc-bottom cellular sample after tensile testing

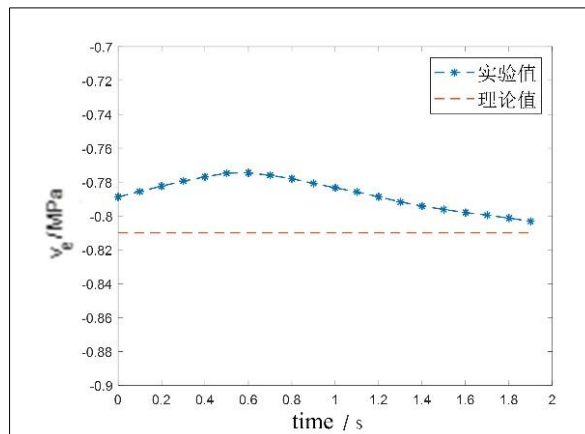
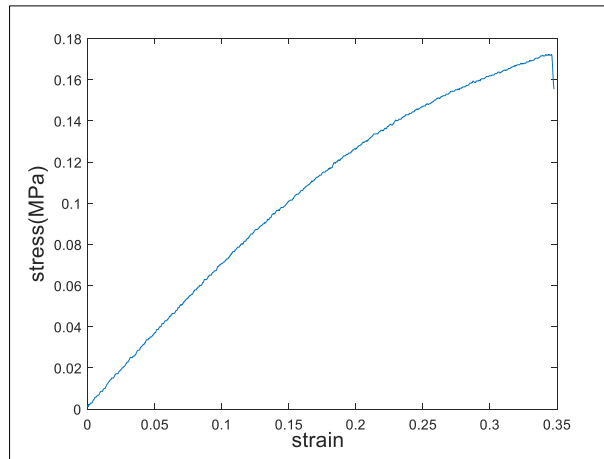


Figure 9 The variation of the equivalent Poisson's ratio of the arrow-shaped concave arc-bottom cellular sample with time during the imaging process



**Figure 10** Stress-strain curve of the arrow-shaped concave arc-bottom cellular sample

Table 2 summarizes the theoretical results and finite element results for the equivalent Poisson's ratio and equivalent elastic modulus of the arrow-shaped concave arc-bottom cellular structure. The data indicate that the theoretical results for both the equivalent Poisson's ratio and equivalent elastic modulus are very close to the experimental results, with average errors for both measurements being less than 2%. The discrepancies between the theoretical and experimental values can be attributed to several factors. First, there may be variations in the elastic modulus of the 3D-printed material, which could influence the tensile performance of the final samples. Second, the calculations for the theoretical values and finite element results did not account for the vertical shear effects caused by constraints between the cellular units. Lastly, during the tensile testing, installation errors may have resulted in the applied tensile force not being perfectly perpendicular to the width direction.

**Table 2** Mechanical Properties of Arrow-Shaped Concave-Arc-Bottom Unit Cells

Mechanical properties	Theoretical results	Finite element analysis result	Experimental Results
$E_e / E$	$3.80 \times 10^{-4}$	$3.81 \times 10^{-4}$	$3.76 \times 10^{-4}$
$\nu_e$	-0.81	-0.81	-0.79

The previous sections have conducted theoretical analysis, finite element analysis, and experimental validation of the equivalent elastic modulus and equivalent Poisson's ratio of the unit cell. However, the mechanical properties of these single unit cells only represent local characteristics and cannot comprehensively reflect the overall performance of the structure after periodic arrangement. To more comprehensively verify the tensile performance of the arrow-shaped concave-arc-bottom negative Poisson's ratio structure, this paper will also conduct experimental validation on the periodic arrangement of the arrow-shaped concave-arc-bottom honeycomb structure. Additionally, to compare the tensile performance differences between this structure and traditional negative Poisson's ratio honeycomb structures, this paper selects star-shaped honeycomb structures and concave hexagonal structures with the same relative density as reference groups for comparison. The dimensions and the number of unit cells for each honeycomb structure are shown in Table 3.

**Table 3** Geometric Parameters of Honeycomb Structures

Sample Shape of Honeycomb Structures	Length(mm)	Width(mm)	Thickness(mm)	number of unit cells
rectangular.	180	160	5	4×6

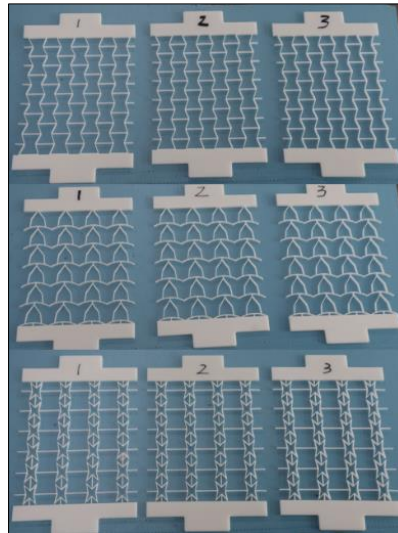


**Figure 11** Honeycomb structure test sample

To evaluate the tensile performance of the samples, a universal testing machine (model WXSA504A), as shown in Figure 6, was used to perform multiple tensile tests on the samples illustrated in Figure 11 at a constant rate of 10 mm/min. During the testing process, the stress-strain curves were recorded, as shown in Figure 12. It can be observed that under continuous loading, the concave hexagonal structure exhibits a greater elastic modulus and load-bearing capacity but fails suddenly; the star-shaped structure enters a significant plastic deformation stage; while the arrow-shaped arch-bottom unit gradually fails, as indicated by multiple linearly fluctuating patterns in the graph. Ultimately, the data were integrated and numerically computed to obtain the equivalent elastic moduli of the three structures, as presented in Table 4.

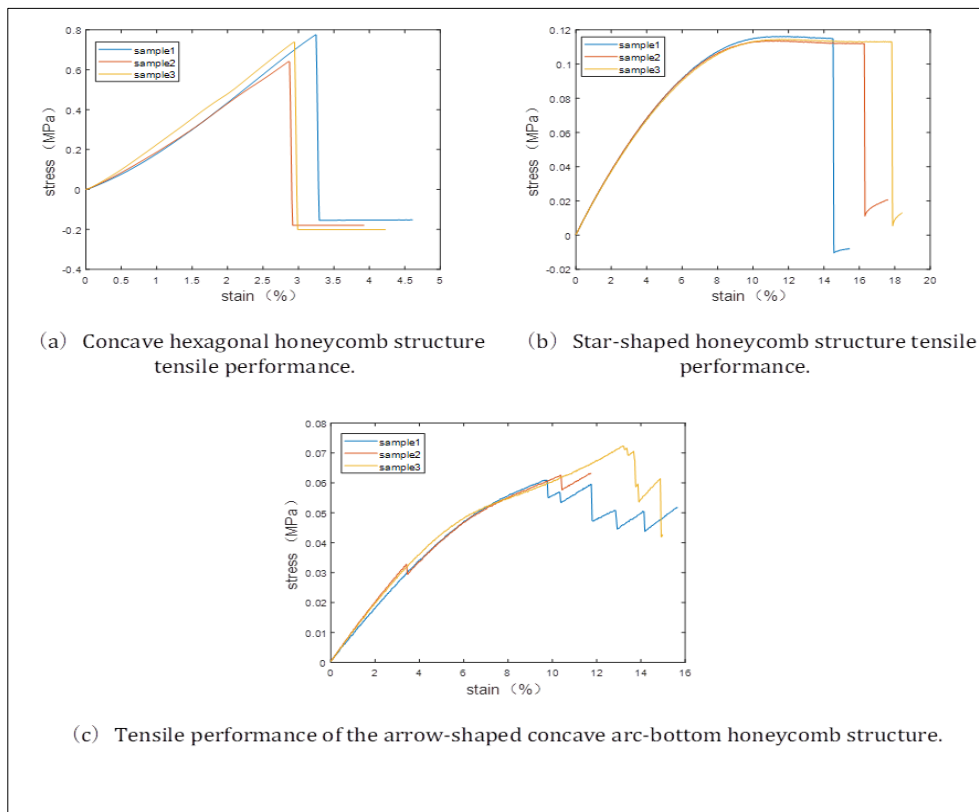


**Figure 12** Stress-strain curves of tensile tests for each honeycomb structure

By comparing with traditional honeycomb structures, the study found that the arrow-shaped arch-bottom honeycomb structure exhibits a lower elastic modulus while requiring less force to achieve a specified deformation. The experimentally measured elastic modulus of this structure is 5.34% of that of the classic concave hexagonal structure.

**Table 4** The experimentally measured equivalent elastic modulus of the three structures

Structure Name	arrow-shaped concave arc-bottom honeycomb structure	Concave hexagonal honeycomb structure	Star-shaped honeycomb structure
$E_y$ (MPa)	1.03	18.88	2.02

## 5. Conclusion

This paper presents a novel arrow-shaped concave-arc-bottom honeycomb structure characterized by significant flexibility and negative Poisson's ratio properties. Utilizing energy methods, the relative density, equivalent elastic modulus, and equivalent Poisson's ratio of this honeycomb structure have been analyzed. The validity of the theoretical derivation of its equivalent mechanical properties has been confirmed through finite element methods and experimental tests. Furthermore, a parametric analysis was conducted to investigate the influence of geometric parameters of the unit cell on the equivalent mechanical properties of the honeycomb structure. The main conclusions drawn from this study are as follows:

- Based on the fundamental assumptions of beam theory, this paper establishes a theoretical model for the arrow-shaped concave-arc-bottom honeycomb structure using the energy principle. The model encompasses the equivalent elastic modulus, equivalent Poisson's ratio, and equivalent density of the topologically optimized structure in the primary impact direction.
- A comparative analysis of the theoretical model was conducted through finite element simulation and experimental methods. The results indicate that the error between the theoretical model and the finite element simulation results is less than 1.5%, while the error with the experimental results is less than 2%. This outcome strongly validates the accuracy and reliability of the established theoretical model.
- By conducting tensile tests on the periodically arranged arrow-shaped concave-arc-bottom honeycomb structure, the results indicate that, compared to traditional negative Poisson's ratio honeycomb structures, the arrow-shaped concave-arc-bottom negative Poisson's ratio honeycomb structure exhibits superior deformation capabilities. The elastic modulus of this structure is only 5.34% of that of the classic concave hexagonal structure

## Compliance with ethical standards

### *Disclosure of conflict of interest*

No conflict of interest to be disclosed.

## References

- [1] Liu Q. Literature review: materials with negative Poisson's ratios and potential applications to aerospace and defence[M]. Victoria, Australia: DSTO, 2006.
- [2] Alderson A, Alderson K L. Auxetic materials[J]. Proceedings of the Institution of Mechanical Engineers, Part G: Journal of Aerospace Engineering, 2007, 221(4): 565-575.
- [3] Prawoto Y. Seeing auxetic materials from the mechanics point of view: A structural review on the negative poisson's ratio[J/OL]. Computational Materials Science, 2012, 58: 140-153.
- [4] Lakes R S. Negative-Poisson's-ratio materials: auxetic solids[J]. Annual review of materials research, 2017, 47: 63-81.
- [5] Lakes R. Deformation mechanisms in negative Poisson's ratio materials: structural aspects[J]. Journal of materials science, 1991, 26: 2287-2292.

- [6] AI Sen, GUO Yuchao, NIE Xiaohua, et al. One-dimensional deformation behavior of a honeycomb structure with zero Poisson's ratio [J]. *Journal of Nanjing University of Aeronautics & Astronautics*, 2021, 53 (4) : 629-636.
- [7] Lakes R. Foam structures with a negative Poisson's ratio[J]. *Science*, 1987, 235(4792): 1038-1040.
- [8] Evans K E, Nkansah M A, Hutchinson I J. Auxetic foams: modelling negative Poisson's ratios[J]. *Acta metallurgica et materialia*, 1994, 42(4): 1289-1294.
- [9] Gibson L J. Cellular solids[J]. *Mrs Bulletin*, 2003, 28(4): 270-274.
- [10] Habib F N, Iovenitti P, Masood S H, et al. In-plane energy absorption evaluation of 3D printed polymeric honeycombs[J]. *Virtual and Physical Prototyping*, 2017, 12(2): 117-131.
- [11] Foo C C, Chai G B, Seah L K. Quasi-static and low-velocity impact failure of aluminium honeycomb sandwich panels[J]. *Proceedings of the Institution of Mechanical Engineers, Part L: Journal of Materials: Design and Applications*, 2006, 220(2): 53-66.
- [12] Zhu F, Zhao L, Lu G, et al. Deformation and failure of blast-loaded metallic sandwich panels—experimental investigations[J]. *International Journal of Impact Engineering*, 2008, 35(8): 937-951.
- [13] Li D, Yin J, Dong L, et al. Strong re-entrant cellular structures with negative Poisson's ratio[J]. *Journal of materials science*, 2018, 53(5): 3493-3499.
- [14] Ren Yiru Jiang HongYong, et al. Crashworthiness of bio-inspired auxetic reentrant honeycomb with negative Poisson's ratio [J]. *ActaAeronautica et Astronautica Sinica*, 2020, 41(23978): 1-11. ( in Chinese).
- [15] Wang Liang, Liu HaiTao, et al. study on tensile mechanical behavior of x-type re-entrant honeycomb structure [J]. *Journal of Mechanical Strength*, 2020, 42(4): 896-900. ( in Chinese).
- [16] Guo ZhiXi, Xiao JunHua, et al. Mechanical properties of multi-arc concave honeycomb structure with adjustable poisson's ratio [J]. *Engineering Mechanics*, 2023, 40(10): 204-212, 236. ( in Chinese).
- [17] Yang H, Ma L. Multi-stable mechanical metamaterials with shape-reconfiguration and zero Poisson's ratio[J]. *Materials & Design*, 2018, 152: 181-190.
- [18] Chang L, Shen X, Dai Y, et al. Investigation on the mechanical properties of topologically optimized cellular structures for sandwiched morphing skins [J]. *Composite Structures*, 2020, 250: 112555.
- [19] Lu Zixing, Wang Huan, Yang ZhenYu et al. In-plane dynamic crushing of star-arrowhead honeycomb structure [J]. *Acta Materiae Compositae Sinica* 2019, 36(08): 1893-1900.
- [20] Leipeng S, Qiang L I, Hongjie W, et al. In-Plane and Out-of-Plane Mechanical Properties of Zero Poisson's Ratio Cellular Structures for Morphing Application[J]. *Transactions of Nanjing University of Aeronautics & Astronautics*, 2022, 39(3).
- [21] Lee M, Niu Z, Slebodnick C, et al. Structure and properties of N, N-alkylene Bis (N'-alkylimidazolium) salts[J]. *The Journal of Physical Chemistry B*, 2010, 114(21): 7312-7319